Nuclear Lattice Effective Field Theory: Status A.D. 2026

Ulf-G. Meißner[1,2,3]

[1] Helmholtz-Institut für Strahlen- und Kernphysik and Bethe Center for Theoretical Physics, Universität Bonn, D-53115 Bonn, Germany
E-mail: meissner@hiskp.uni-bonn.de

[2] Institute for Advanced Simulation (IAS-4). Forschungszentrum Jülich, D-52425 Jülich, Germany

[3] Cluster of Excellence - Color meets Flavor (CmF)

I discuss recent developments in nuclear lattice effective field theory, which is a premier tool in the theory of nuclear structure and reactions. Topics include the search for the tetraneutron, multi-neutron correlations in light nuclei, the radii of selected oxygen isotopes, the tin isotopes close to the proton drip line and a number of scattering processes (n-α, d-d and α-α).

1 Introduction

The matter surrounding us is made of atomic nuclei and the emergence of these strongly interacting particles is one of the last open issues for the immensely successful Standard Model of particle physics. Much progress in the understanding of the structure and dynamics of nuclei has been made in the context of Nuclear Lattice Effective Field Theory (NLEFT) [1], which combines the so successful low-energy chiral effective field theory of QCD with stochastic methods (Monte Carlo simulations). While direct calculations of nuclei based on quarks and gluons in the framework of lattice QCD are essentially impossible due to the severe sign problem, formulating the nuclear forces in terms of protons, neutrons and pions is not only more appropriate, but also comes with the added value of the approximate Wigner SU(4) (spin-isospin) symmetry of the underlying nuclear interactions. This symmetry in fact suppresses the sign oscillations strongly, and in the limit of an exact Wigner SU(4) symmetry, spin-isospin saturated nuclei like e.g. ^{4}He are free of any sign oscillation. A further suppression of these sign oscillations is achieved through the so-called wavefunction matching, introduced in Ref. [2]. In NLEFT simulations, Euclidean space-time is discretized on a torus of volume $L^3 \times L_t$, where L is the side length of the spatial dimension, and L_t denotes the extent of the Euclidean time dimension. The lattice spacing in the spatial (temporal) dimensions is a (a_t). Throughout, we work in the Hamiltoinan limit of a very small a_t, typically $a_t = 1/(1000\,\mathrm{MeV})$, see e.g. the discussion in Ref. [3]. The maximal momentum on the lattice is $p_{\max} \equiv \pi/a$, which serves as the UV regulator of the theory. Nucleons are point-like particles on the lattice sites, and the interactions between nucleons (pion exchanges and contact terms) are treated as insertions on the nucleon world lines via auxiliary-field representations. Properties of multi-nucleon systems are computed by means of the projection Monte Carlo (MC) method. Each nucleon is treated as a single particle propagating in a fluctuating background of pion and auxiliary fields. Both local and non-local smearings are applied to the nucleon creation and annihilation operators. Euclidean time projection is started from some initial state Ψ_A for Z protons and N neutrons (with $A = Z + N$). One calculates the ground state energy and other properties from the correlation function $Z(t) \equiv \langle \Psi_A | \exp(-tH) | \Psi_A \rangle = \mathrm{Tr}\{M^{L_t}\}$, in the limit of large Euclidean projection time t, with M the normal-ordered transfer-matrix operator and L_t the number of Euclidean time steps. Higher-order contributions are computed as perturbative corrections to the LO results. A much more detailed description is given in the monograph [1] and a recent review is Ref. [4].

2 Searching for the tetraneutron on the lattice

Bound nuclear systems conventionally form when protons and neutrons coalesce through the strong interaction. However, the combination of attractive strong interactions and the absence of Coulomb repulsion makes the existence of pure neutron nuclei a plausible concept, a quest that dates back to the early 1960s. Confirming or ruling out the existence of such neutral nuclei, whether as bound or resonant states, is crucial for advancing our understanding of nuclear physics, the strong interaction, universal fermion properties in the unitary limit, and astrophysical objects. Substantial experimental and theoretical efforts have been dedicated to this challenge. In 2002, events characteristic of multineutron clusters were observed in the breakup of ^{14}Be [5]. In 2016, a candidate resonant tetraneutron ($4n$) state with an energy of 0.83 ± 0.65(stat.) $\pm\, 1.25$(syst.) MeV was reported in the missing-mass spectrum of the ^{4}He(^{8}He,^{8}Be)$4n$ reaction [6]. Most notably, a recent high-statistics experiment on the ^{8}He(p,p^4He)$4n$ reaction observed a clear peak structure near the threshold at 2.37 ± 0.38(stat.) $\pm\, 0.44$(syst.) MeV [7]. While a bound $4n$ nucleus is generally believed to be excluded, the interpretation of these signals as a resonance remains highly debated. The low-energy peak observed by [7] has been explained as a consequence of dineutron-dineutron correlations through a reaction model study [8]. However, there is a number of calculations that have reported a low-lying $4n$ resonance with energies and widths close to the experimental values.

To further elucidate the nature of the $4n$ signal reported in [7], additional theoretical investigations are needed. In Ref. [9] we have studied the $4n$ system using NLEFT. employing both a simpler SU(4) and the high-fidelity N^{3}LO interaction. In the left panel of Fig. 1 the calculated energy of the tetraneutron system at different L values, using both the full N^{3}LO interaction ($a = 1.32$ fm) and the simple SU(4) interaction ($a = 1.64$ fm) is shown. Indicated are also the candidate resonance energies from experimental studies: $E = 2.37 \pm 0.38$(stat.) $\pm\, 0.44$(syst.) MeV from Ref. [7] and $E = 0.83 \pm 0.65$(stat.) $\pm\, 1.25$(syst.) MeV from Ref. [6]. For comparison, the energies of the $2n$ system at different L values using the SU(4) and N^{3}LO interactions are computed via the Lanczos eigenvector method, which eliminates Monte Carlo and extrapolation uncertainties. Both the N^{3}LO and SU(4) interactions yield similar results for the $4n$ system, showing strongly repulsive behavior at small L due to Pauli blocking, with energies gradually decreasing as L increases. This consistency confirms earlier findings that the tetraneutron system is insensitive to details of the nuclear interaction as long as it is realistic. The smooth, continuous decrease of the $4n$ energy lacks the characteristic plateau formation expected for resonances in finite-volume methods, suggesting a behavior typical of a non-bound system that does not form a resonance. We now turn to the extraction of the

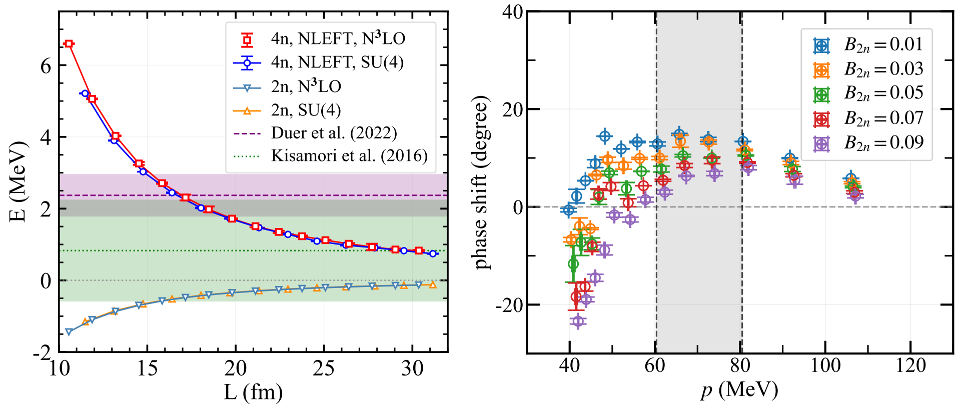

Figure 1. **Left panel:** Ground-state energies of the $4n$ system calculated using NLEFT with both $\mathrm{N^3LO}$ and SU(4) interactions, and the $2n$ system calculated using the Lanczos eigenvector method with the SU(4) interaction, as functions of the lattice size L. The error bars of NLEFT results indicate the uncertainty from the extrapolation. **Right panel:** Dineutron-dineutron S-wave scattering phase shift δ as a function of relative momentum p extracted from finite-volume $4n$ and $2n$ energies using Lüscher's method and the composite-dimer finite-volume relation for the $\mathrm{N^3LO}$ chiral EFT interaction of Ref. [2]. Different symbols correspond to the scanned near-threshold values of B_{2n} (in MeV), and the shaded band indicates the momentum range associated with $L \simeq$ 20–15 fm.

S-wave $2n$-$2n$ phase shifts from our finite-volume spectra. For the realistic $\mathrm{N^3LO}$ chiral EFT Hamiltonian of Ref. [2], the infinite-volume two-neutron system is not bound, but it corresponds to a virtual state. Nevertheless, in the periodic boxes used here the lowest nn S-wave level is shifted below the two-neutron threshold and can be treated as a shallow finite-volume dimer (a quasi-bound dineutron). This provides a practical intermediate description in which the four-neutron finite-volume levels are interpreted as two composite dimers in relative motion, and Lüscher's relation can be used to map the discrete energies to elastic $2n$-$2n$ phase shifts $\delta(p)$. The resulting $2n$-$2n$ S-wave phase shifts are shown in the right panel of Fig. 1. In the intermediate window $p \simeq$ 55–100 MeV, $\delta(p)$ displays a clear non-monotonic structure, indicating a weak attractive feature. However, we do not observe the characteristic rapid rise through 90° that would signal a narrow elastic resonance. In the future, we plan to extend the NLEFT framework to investigate the $^8\mathrm{He}(p, p^4\mathrm{He})4n$ reaction and understand the correlated structures observed.

3 Multi-neutron correlations in light nuclei

The quest to understand multi-neutron systems has a long history and recent experimental efforts aim to probe candidate four-neutron configurations in neutron-rich light nuclei such as ^{8}He and ^{7}H via quasi-free knockout reactions, see Ref. [10] for a review. However, the ground-state energies of the hydrogen isotopes ^{6}H and ^{7}H are not yet well constrained, with substantial discrepancies across experimental analyses and theoretical predictions. Using *ab initio* NLEFT with an ensemble of 282 chiral two- and three-nucleon forces, in Ref. [11] we have performed an uncertainty-quantified analysis of the ground-state (g.s.) energies of ^{6}H and ^{7}H, finding $E_{\mathrm{g.s.}} = -4.94(0.14)$ MeV and $-5.29(0.16)$ MeV, respectively, see Fig. 2 (left panel). The marginal posteriors suggest single-neutron separation energy

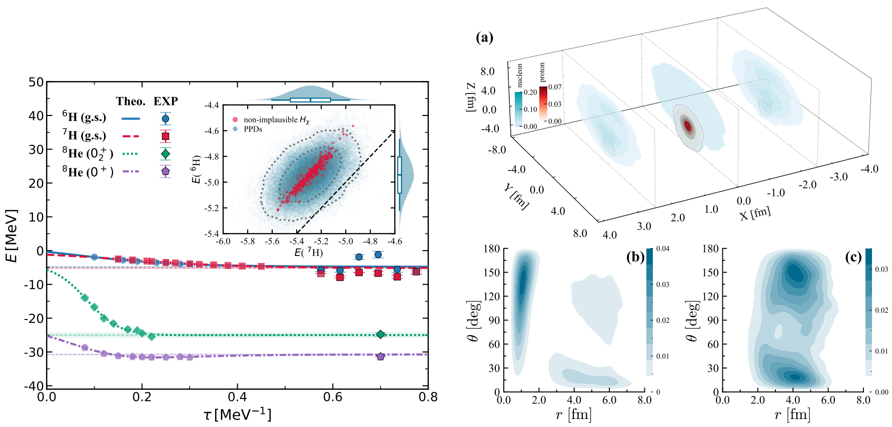

Figure 2. **Left panel:** Calculated and experimental g.s. energies of ^{6,7}H, and the 0^+ and ${0_2}^+$ state energies of ^{8}He. Colored markers overlaid on the corresponding curves indicate the calculated energies versus Euclidean time τ, with statistical uncertainties. The curves represent the τ-extrapolation fits, and horizontal dashed lines denote the extrapolated $\tau \to \infty$ energies with their statistical uncertainties. Experimental data are shown as symbols labeled "EXP" in the legend. **Inset:** The red circles represent the g.s. energies of ^{6,7}H from non-implausible prior samples obtained via history matching, including uncertainties. Posterior samples are shown as pale blue points, with dashed lines indicating the 1σ and 2σ credible intervals. The dashed black line denotes the condition $E(^6\text{H}) = E(^7\text{H})$. Marginal distributions are shown along each axis, with medians indicated by ticks and thick and thin bars representing the 1σ and 2σ credible intervals, respectively. **Right panel:** (a) Intrinsic nucleon (blue) and proton (red) densities of the ^{7}H ground state, visualized as slices at $x = 0$ and $x = \pm 2.5$ fm. The red dashed line marks the maximal spatial extent of the identified triton cluster. (b) Two-neutron correlation density of all neutrons in the ^{7}H ground state, with r defined relative to the center-of-mass (c.m.) of the core. (c) Two-neutron correlation density of the four valence neutrons, with r defined with respect to the c.m. of the ^{7}H.

$S_n(^7\text{H}) = 0.35 \pm 0.32$ MeV, disfavoring sequential $^6\text{H} + n$ decay and pointing towards direct $t + 4n$ emission. Intrinsic densities indicate triton- and α-like clusters in ^{7}H and ^{8}He, respectively. By computing two-body and reduced four-body correlation functions, we find that the valence neutrons in the surface region of these systems form compact dineutrons that predominantly organize into symmetric dineutron-dineutron configurations, with only a small but non-negligible fraction assembling into more compact tetraneutron-like substructures, see Fig. 2 (right panel). In ^{7}H, these components account for roughly 95% and 5% of the sampled four-neutron configurations, respectively, and ^{8}He exhibits a similar hierarchy. For these configurations, we also extract the corresponding spatial and angular correlation patterns among the nucleons. These results provide nuclear-structure insights into the debate surrounding four-neutron clusters and complement ongoing experimental searches for tetraneutron signatures in light nuclei.

4 Radii of selected oxygen isotopes

Accurate *ab initio* predictions of nuclear charge and matter radii remain a long-standing challenge in nuclear theory, owing to strong many-body correlations and severe Monte Carlo sign problems, see e.g. Refs. [12]–[14]. In our earlier work, we had already shown that within NLEFT using the wave-function matching apporach [2], this problem is over-

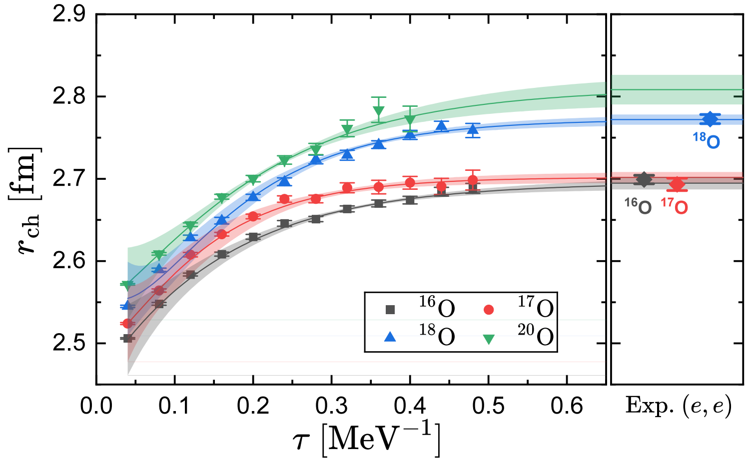

Figure 3. Results for the charge radii for the oxygen isotope chain compared to experiment. The radius of ^{20}O is a prediction (green line/band). Here, τ is the Euclidean time. For more details, see Ref. [16].

come, but the accuracy of some predictions for the charge radii needed improvement due to the sign problem induced by the pinhole algorithm. The latter is the tool to fix the center-of-mass on the lattice and thus allows to calculate the charge distributions and the pertinent moments, like the radii. For details, see Refs. [2], [15]. In Ref. [16], we have addressed this challenge for part of the oxygen isotopic chain by performing first-principles calculations of the charge and matter radii of $^{16\text{–}20}$O within NLEFT using high-fidelity chiral interactions at next-to-next-to-next-to-leading order (N^{3}LO). To overcome the prohibitive sign oscillations encountered in conventional radius calculations, we introduce the *partial pinhole algorithm*, which systematically reduces the rank of the many-body density operator and enables stable simulations at significantly larger imaginary times. By combining the partial pinhole algorithm with the wave-function matching method, we achieve a substantial reduction of statistical uncertainties and are able to resolve subtle isotopic trends in nuclear radii. Our results accurately reproduce the experimentally observed charge radii of ^{16}O, ^{17}O, and ^{18}O, including the pronounced increase from ^{17}O to ^{18}O that has remained elusive in other *ab initio* approaches, see Fig. 3. Furthermore, we provide a first-principles prediction for the charge radius of the neutron-rich isotope ^{20}O, $r_{\mathrm{ch}}(^{20}\mathrm{O}) = 2.810(32)$ fm. The calculated matter radii show excellent agreement with values extracted from low-energy electron and proton scattering, while revealing significant discrepancies with those inferred from interaction cross sections, thereby highlighting model-dependent ambiguities in experimental extractions.

5 Lattice calculation of the proton-rich tin isotopes

The ^{100}Sn isotope is a particularly fascinating nucleus. It is a rare example of a doubly magic nucleus with equal proton and neutron numbers, $Z = N = 50$, and it sits close to the proton dripline of the extensive tin isotopic chain. It also exhibits among the largest known allowed β-decay strengths and features enhanced α decays. These features make it central to both studies of nuclear structure and astrophysical nucleosynthesis. The neigh-

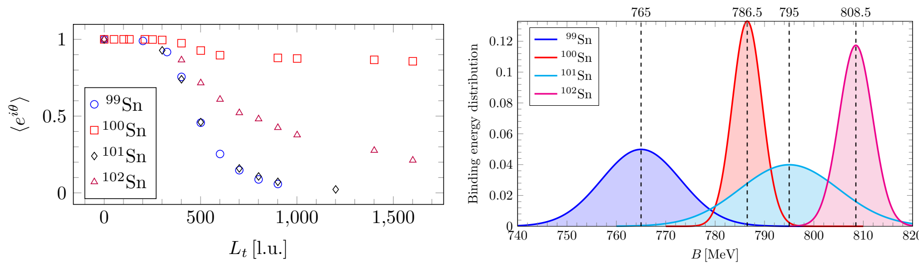

Figure 4. **Left panel:** The average phase $\langle e^{i\theta} \rangle$ as a function of time steps L_t for the Sn isotopes considered here. **Right panel:** Distribution of the obtained binding energies B for ^{99}Sn – ^{102}Sn. The central values are indicated by the dashed black lines and given on the top axis of the plot.

boring isotopes ^{99}Sn, ^{101}Sn, and ^{102}Sn are equally important and pose formidable challenges to *ab initio* nuclear theory, where weak binding, continuum coupling, and Coulomb effects amplify the impact of many-body truncations and the calibration of three-nucleon (3N) forces. Few regions of the nuclear chart combine such a sharp theoretical challenge with equally rapid experimental progress. Recent advancements at radioactive-ion-beam facilities have enabled high-precision mass measurements, decay spectroscopy, and spectroscopic studies of ^{100}Sn and nearby isotopes, offering stringent benchmarks for modern nuclear interactions. These developments highlight the urgent need for theoretical frameworks that can treat medium-to-heavy exotic nuclei from first principles.

With the advent of exascale computational capabilities now available with JUPITER at Forschungszentrum Jülich [17], it has become feasible to extend these investigations into the region of nuclei with $A \simeq 100$ in Ref. [18]. We could perform lattice calculations of the ground-state energies of the proton-rich isotopes $^{99–102}$Sn closest to the assumed proton dripline. We employ NLEFT with high-fidelity chiral interactions at N^{3}LO, as developed in Ref. [2]. The dependence of the corresponding average complex phase

$$\langle e^{i\theta} \rangle = \langle \det(\mathcal{M}_{L_t}) / |\det(\mathcal{M}_{L_t})| \rangle \, , \tag{1}$$

with $\mathcal{M}_{L_t}$ the transfer matrix product up to Euclidean time L_t, is depicted in the left panel of Fig. 4. Not unexpectedly, the phase of the even–odd nuclei is decreasing significantly faster than the one for even–even nuclei, yet there is still a sufficiently strong signal to precisely extract the corresponding ground state energies of ^{99}Sn and ^{101}Sn. The extracted energies are displayed in the right panel of Fig. 4. For all isotopes, calculations with the original N^{3}LO Hamiltonian systematically underbind by about 5% relative to experiment. This is not unexpected, as the three-nucleon forces were originally constrained in the light-to-medium mass region up to ^{40}Ca. It is known that these 3NFs are more attractive for heavier systems, as already seen and discussed in the study of nuclear matter in Ref. [2]. To assess the role of three-nucleon forces, we performed controlled variations of two SU(4)-symmetric 3N couplings, originally motivated by α-cluster EFT. With only a percent-level adjustment, we reproduce the experimental binding energy of ^{100}Sn and find for the other three isotopes agreement with experiment: E(^{99}Sn)= $804(8)[807.9(0.6)]$, E(^{101}Sn)= $834(10)[836.4(0.3)]$, and E(^{102}Sn)= $848.1(3.4)[849.1(0.1)]$, with all values in MeV and the empirical values in the square brackets. Importantly, this adjustment retains the good description of the nuclei reported in the original fit. The corresponding mass splittings and two-neutron separation energies agree well with experiment, although

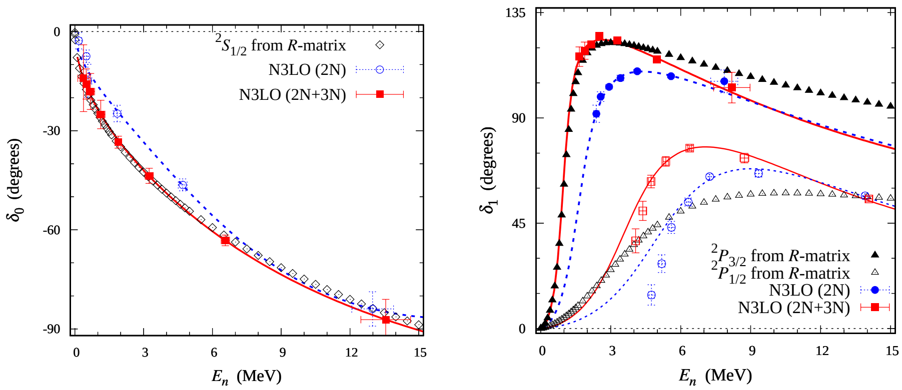

Figure 5. Neutron-alpha phase shifts at N^{3}LO as functions of the neutron laboratory energy E_n. **Left panel:** $^2S_{1/2}$. **Right panel:** $^2P_{3/2}$ and $^2P_{1/2}$. Symbols with error bars are lattice results, blue circles denote the N^{3}LO (2N only) results, and red squares denote N^{3}LO (2N+3N) results. Solid red curves are effective range expansion (ERE) fits to the full N^{3}LO (2N+3N) lattice data, and dashed blue curves are ERE fits to the the N^{3}LO (2N sole) lattice points. Black symbols denote empirical R-matrix phase shifts [26] (diamonds for $^2S_{1/2}$ and filled and open triangles for $^2P_{3/2}$ and $^2P_{1/2}$).

the uncertainties are still too large, but this is not surprising since this was a pioneering calculation to investigate whether this mass region is at all accessible to NLEFT. For an NLEFT study of ^{100}Sn using SU(4)-symmetric forces supplemented with a spin-orbit interaction, see Ref. [19].

6 Scattering processes in NLEFT

Scattering processes on the lattice require special methods. Most famous is the Lüscher approach, which relates the continumm phase shift to the volume dependence of the energy levels measured on the lattice [20]. In NLEFT, the spherical wall technique [21], [22] and its extension using an auxiliary potential [23] are frequently used as they are more precise. For scattering involving clusters, the adiabatic projection method (APM) is the method of choice [24], [25]. All these methods will be employed in the reactions to be discussed next.

6.1 Ab initio lattice study of neutron-alpha scattering with chiral forces at N^{3}LO

It is well established that neutron-alpha (n-α) scattering is a fine probe of three-nucleon forces that play such an important role in precision calculations of atomic nuclei, see e.g. Ref. [27]. The first *ab initio* lattice calculation of n-α scattering employing NLEFT with chiral interactions up to next-to-next-to-next-to-leading order (N^{3}LO) was presented in Ref. [28]. By utilizing the high-fidelity chiral Hamiltonian developed in our previous work, we computed scattering phase shifts in the S- and P-wave channels via the Lüscher finite-volume method [20]. Our findings show excellent agreement with empirical R-matrix analyses in the $^2S_{1/2}$ and $^2P_{3/2}$ channels, see Fig. 5 (left panel). while highlighting persistent discrepancies in the $^2P_{1/2}$ channel at neutron energies above $E_n \simeq 5$ MeV, see also Fig. 5 (right panel). We systematically investigated these discrepancies using a simplified neutron-alpha model, confirming that the issue is not due to methodological limitations of the Lüscher approach. Furthermore, we revisit and refine our three-nucleon force (3NF) parameterization procedure by explicitly incorporating neutron-alpha scattering data, underscoring the stability of nuclear binding-energy predictions and identifying areas for further refinement of lattice three-nucleon forces. This comprehensive analysis provides significant benchmarks for state-of-the-art *ab initio* nuclear theories and advances our understanding of nucleon-nucleus scattering processes, particularly emphasizing the importance of accurately formulating three-nucleon forces in nuclear lattice calculations.

6.2 Elastic deuteron-deuteron scattering within NLEFT

Big bang nucleosynthesis (BBN) works as an excellent probe of physics beyond the Standard Model as it is the first process in the history of the early universe that is well understood. Measurements for primordial element abundances are getting more and more precise. In order to have reliable theoretical predictions for BBN that can be compared to observations it is crucial to know the dominant reaction rates precisely. In Ref. [29], the significance of the deuteron-deuteron reactions $d(d,n)^3\mathrm{He}$ and $d(d,p)^3\mathrm{H}$ for the accuracy of theoretical BBN predictions was laid out. Within the framework of NLEFT one can calculate the reaction rates for $d(d,n)^3\mathrm{He}$ and $d(d,p)^3\mathrm{H}$ *ab initio*. As a first step towards calculating these rates, we have considered in Ref. [30] the single-channel $d+d$, ${}^5S_2$ scattering problem. Because the deuteron is weakly bound and its wave function thus broad, treating two deuterons on a confined lattice is demanding and requires a careful analysis. We choose a rather large box of length $L = 18.4\,\mathrm{fm}$ to minimize finite-volume effects. We determine that the threshold energy obtained by simulating two non-interacting deuterons on the lattice is consistent within uncertainties with twice the true deuteron ground state energy when extrapolating to infinite Euclidean time, see the left panel of Fig. 6. We obtain $E_\infty = -1.331(3.263)$ MeV. On the fine lattice with $a = 1.32\,\mathrm{fm}$ used here, the norm matrix appearing in the adibatic Hamiltonian requires regularization as the lowest eigenvalues are exteremly noisy. We have used both the Tikhonov regularization [31] as well as the truncated SVD regularization (norm matrix projection). Our results for the ${}^5S_2$ phase shift are shown in the right panel of Fig. 6. First, the results obtained with the two norm-matrix regularization methods agree within their uncertainties. Second, our phase shifts become more negative at increasing momentum than those reported in Refs. [32]–[36] corresponding to stronger effective repulsion. The three-nucleon interactions have only a small effect, and omitting them makes the phase shifts slightly less negative. Correspondingly, we find larger ERE parameters than reported earlier. We get ${}^5a_{dd} = 12.96(0.26)$ fm and ${}^5r_{dd} = 3.62(0.79)$ fm for the scattering length and effective range, respectively This calculation establishes the feasibility of treating the $d+d$, ${}^5S_2$ channel with NLEFT and identifies the numerical requirements for extending the calculation to coupled reaction channels.

6.3 *Ab initio* α–α scattering with high-fidelity chiral interactions

The elastic scattering of two α particles is one of the most fundamental processes in low-energy nuclear physics. The ^{8}Be system it probes is unbound, decaying back into two α particles, yet its narrow 0^+ ground-state resonance just above the α–α threshold and its broad 2^+ first excited state are the gateway to almost all helium burning in stars. The

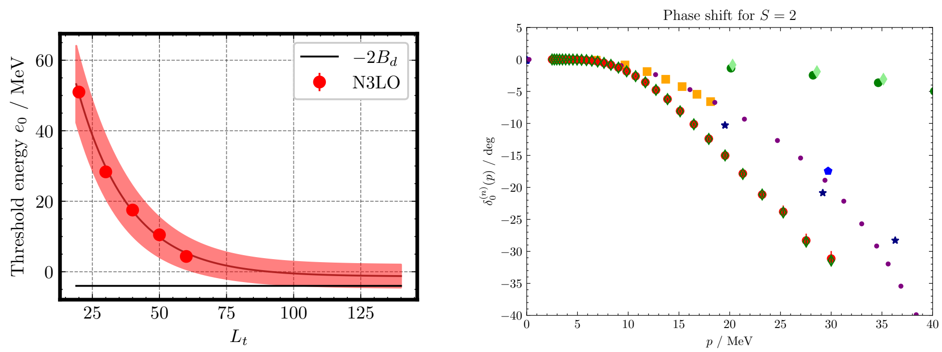

Figure 6. **Left panel:** Threshold energy of two non-interacting deuterons on the lattice as a function of Euclidean time L_t. The red band shows the result from an exponential fit, the red dashed line is the expected result of twice the deuteron binding energy at N^{3}LO. **Right panel:** Coulomb-subtracted phase shift of the projected single-channel $d + d$ elastic scattering phase shift for the $^5S_2$ channel from NLEFT at N^{3}LO in the chiral expansion with the Tikhonov regularization (green empty diamonds) and with the norm mode projection method (red circles) compared to results from the literature using different continuum methods [32]–[36].

triple-α process proceeds through the unstable ^{8}Be ground state followed by radiative capture of a third α particle into the Hoyle state of ^{12}C, and subsequent α captures generate the nuclear "ash" of O, Ne, and heavier elements that shape stellar evolution and type-Ia supernovae. Because the ^{8}Be resonances are imprinted directly on the α–α phase shifts, elastic scattering provides a clean, parameter-free benchmark for any microscopic theory of α-cluster dynamics [37]. *Ab initio* nuclear theory has made striking progress on light-nucleus reactions over the past two decades, but almost always with a light probe on a light target. NLEFT occupies a complementary niche. Its mild computational scaling, combined with the APM, formulated directly in terms of composite two-cluster states, enabled the first *ab initio* study of α–α scattering [38] and defines a route that scales favorably toward the heavier α-cluster reactions, such as triple-α and radiative α capture, that forge carbon and oxygen in evolved stars. However, the pionnering calculation reported in Ref. [38] was performed on a coarse lattice ($a = 1.97$ fm) and with the N^{2}LO legacy action. As noted in the previous subsection, on a fine lattice and using the high-fidelity N^{3}LO interaction, the norm matrices require some type of regularization [39]. As in the case of d-d scattering, we used both the Tikhonov and the truncated SVD regularization for calculating the α-α phase shift, shown in Fig. 7. The S-wave phase shift begins near $180°$ at threshold—reflecting the deeply bound Pauli-forbidden configurations of the eight-nucleon system, in accordance with Levinson's theorem—and decreases smoothly with energy. The D-wave phase shift rises from zero through $90°$ near the ^{8}Be 2^+ resonance. In both partial waves, the lattice results track the empirical phase shifts across the energy range studied, with no adjustable scattering parameters. An effective-range-expansion (ERE) fit to the D-wave yields the resonance parameters $E_R = 3.25(25)$ MeV and $\Gamma_R = 0.75(25)$ MeV, in reasonable agreement with the empirical values $E_R = 2.92(18)$ MeV and $\Gamma_R = 1.34(50)$ MeV [37]. This represents a significant improvement over the N^{2}LO analysis of Ref. [38]. The agreement of the NLEFT prediction with the data is good but not yet perfect, and the residual discrepancies point to a refinement of the three-nucleon interaction. Guided by the same tension in the n–α system, see subsection 6.1, we are revisiting the 3N forces, and a future α–α calculation with the improved force should sharpen the comparison with the empirical

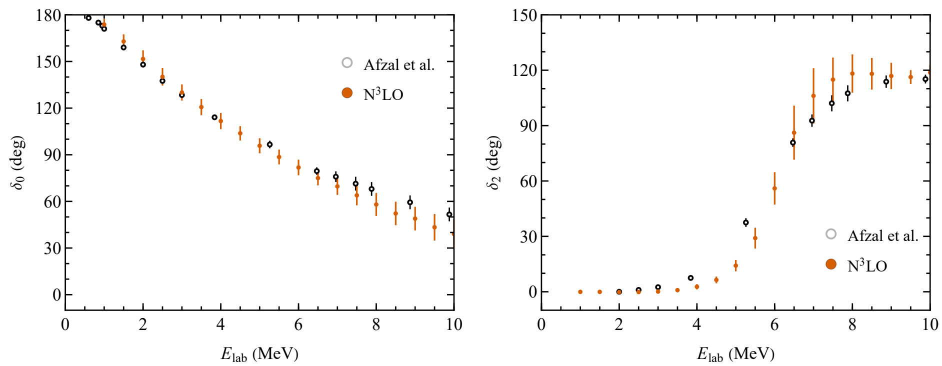

Figure 7. **Left panel:** S-wave α–α phase shift versus laboratory energy. Open circles: empirical phase shifts [37]. Filled circles: current N^{3}LO lattice (theory) results, using Tikhonov regularization, with regulator removed by extrapolation. Theory error bars are jackknife estimates. **Right: panel** D-wave α–α phase shift versus laboratory energy. The phase shift passes through 90° near the 2^+ resonance of ^{8}Be.

phase shifts.

7 Outlook

Finally, let me mention a few on-going projects. First, we are performing systematic studies to better pin down the three-nucleon forces. Second, we started a systematic study of nuclear β-decays. A the first benchmark calculation on the the triton lifetime was published in Ref. [40]. We obtained $\langle F\rangle = 0.99949(11)$ and $\langle GT\rangle = 1.6743(58)$ for the Fermi and the Gamov-Teller matrix element, respectively. This is consistent with other determinations and lays the groundwork for future studies aimed at achieving high-precision predictions for a wide range of nuclear phenomena. Here, we mention in particular the anomlaously long lifetime of ^{14}C, $\tau(^{14}\mathrm{C}) \simeq 5730$ years, which is the backbone of radiocarbon dating. Third, with the available exascale capabilities, we will be able to make predictions for the radii (and other observables) for not only the proton-rich but also the neutron-rich Sn isotopes. Related to this is the puzzling behaviour of the measured charge radii of the Ca isotopes, that so far has to been elusive to *ab initio* nuclear theory. NLEFT is also contributing to the precision extraction of nuclear radii using laser spectroscopy methods, see e.g. Refs. [41], [42]. Fourth, we have also started to combine NLEFT results for nuclear shapes with Monte Carlo Glauber methods, that allow to investigate deformation effects and signals of clustering in nucleus-nucleus collisions at energies of a few hundreds of MeV per nucleon, see e.g. Refs. [43], [44]. Last but not least, first steps towards precision calculations of neutron star properties have been taken in Ref. [45] which are of utmost importance in the multi-messenger area.

Acknowledgements

I thank my NLEFT colleagues for their contributions to the results presented here. The work reported here is part of the ERC AdG EXOTIC supported by the European Research Council (ERC) under the European Union's Horizon 2020 research and innovation programme (grant agreement No. 101018170). This work was also supported in part by the

Deutsche Forschungsgemeinschaft (DFG) under Germany's Excellence Strategy – EXC 3107 – Project-ID 533766364, and from the CAS President's International Fellowship Initiative (PIFI) under Grant No. 2025PD0022. The computational resources were provided by the Jülich Supercomputing Centre (JSC) at Forschungszentrum Jülich. Special resources on the JURECA-DC supercomputer at the JSC and on JUPITER within the JUREAP program are particularly acknowledged.

References

[1] T. A. Lähde and U.-G. Meißner, *Nuclear Lattice Effective Field Theory: An introduction*. Springer, 2019, **957**, ISBN: 978-3-030-14187-5. DOI: 10.1007/978-3-030-14189-9.

[2] S. Elhatisari *et al.*, *Wavefunction matching for solving quantum many-body problems*, Nature, **630**, no. 8015, pp. 59–63, 2024. DOI: 10.1038/s41586-024-07422-z.

[3] Z.-W. Niu, B.-N. Lu, S. Zhang, Y.-Z. Ma, S. Elhatisari, D. Lee, and U.-G. Meißner, *Full Uncertainty Quantification of Sign-Problem-Free Quantum Monte Carlo Methods and Nuclear Lattice Effective Field Theory Benchmarks*, Jul. 2026. [Online]. Available: https://arxiv.org/abs/2607.06044.

[4] D. Lee, *Lattice Effective Field Theory Simulations of Nuclei*, Ann. Rev. Nucl. Part. Sci., **75**, no. 1, pp. 109–128, 2025. DOI: 10.1146/annurev-nucl-101918-023343.

[5] F. M. Marques *et al.*, *The Detection of neutron clusters*, Phys. Rev. C, **65**, p. 044 006, 2002. DOI: 10.1103/PhysRevC.65.044006.

[6] K. Kisamori *et al.*, *Candidate Resonant Tetraneutron State Populated by the He4(He8,Be8) Reaction*, Phys. Rev. Lett., **116**, no. 5, p. 052 501, 2016. DOI: 10.1103/PhysRevLett.116.052501.

[7] M. Duer *et al.*, *Observation of a correlated free four-neutron system*, Nature, **606**, no. 7915, pp. 678–682, 2022. DOI: 10.1038/s41586-022-04827-6.

[8] R. Lazauskas, E. Hiyama, and J. Carbonell, *Low Energy Structures in Nuclear Reactions with 4n in the Final State*, Phys. Rev. Lett., **130**, no. 10, p. 102 501, 2023. DOI: 10.1103/PhysRevLett.130.102501.

[9] L. Wu, S. Elhatisari, U.-G. Meißner, S. Shen, L.-S. Geng, and Y. Kim, *Searching for the Tetraneutron Resonance on the Lattice*, Phys. Rev. Lett., **136**, no. 14, p. 142 502, 2026. DOI: 10.1103/89w9-p443.

[10] F. M. Marqués and J. Carbonell, *The quest for light multineutron systems*, Eur. Phys. J. A, **57**, no. 3, p. 105, 2021. DOI: 10.1140/epja/s10050-021-00417-8.

[11] S. Zhang, S. Elhatisari, and U.-G. Meißner, *Multi-neutron correlations in light nuclei via ab-initio lattice simulations*, Dec. 2025. [Online]. Available: https://arxiv.org/abs/2512.18849.

[12] A. Cipollone, C. Barbieri, and P. Navrátil, *Chiral three-nucleon forces and the evolution of correlations along the oxygen isotopic chain*, Phys. Rev. C, **92**, no. 1, p. 014 306, 2015. DOI: 10.1103/PhysRevC.92.014306.

[13] V. Lapoux, V. Somà, C. Barbieri, H. Hergert, J. D. Holt, and S. R. Stroberg, *Radii and Binding Energies in Oxygen Isotopes: A Challenge for Nuclear Forces*, Phys. Rev. Lett., **117**, no. 5, p. 052 501, 2016. DOI: 10.1103/PhysRevLett.117.052501.

[14]P. Maris *et al.*, *Nuclear properties with semilocal momentum-space regularized chiral interactions beyond N2LO*, Phys. Rev. C, **106**, no. 6, p. 064 002, 2022. DOI: 10.1103/PhysRevC.106.064002.
[15]S. Elhatisari, E. Epelbaum, H. Krebs, T. A. Lähde, D. Lee, N. Li, B.-n. Lu, U.-G. Meißner, and G. Rupak, *Ab initio Calculations of the Isotopic Dependence of Nuclear Clustering*, Phys. Rev. Lett., **119**, no. 22, p. 222 505, 2017. DOI: 10.1103/PhysRevLett.119.222505.
[16]Z. Ren, S. Elhatisari, and U.-G. Meißner, *Ab Initio Study of the Radii of Oxygen Isotopes*, Phys. Rev. Lett., **135**, no. 15, p. 152 502, 2025. DOI: 10.1103/y6s2-43ym.
[17]*Jülich Supercomputing Centre: JUREAP - Seeding Exascale in Europe*, 2025. [Online]. Available: https://www.fz-juelich.de/en/ias/jsc/jupiter/jureap.
[18]F. Hildenbrand, S. Elhatisari, U.-G. Meißner, H. Meyer, Z. Ren, A. Herten, and M. Bode, *Lattice Calculation of the Sn Isotopes near the Proton Dripline*, Phys. Rev. Lett., **136**, no. 6, p. 062 501, 2026. DOI: 10.1103/n7nt-s64t.
[19]Z.-W. Niu and B.-N. Lu, *Sign-Problem-Free Nuclear Quantum Monte Carlo Simulation*, Phys. Rev. Lett., **135**, no. 22, p. 222 504, 2025. DOI: 10.1103/pn99-6dxt.
[20]M. Lüscher, *Two particle states on a torus and their relation to the scattering matrix*, Nucl. Phys. B, **354**, pp. 531–578, 1991. DOI: 10.1016/0550-3213(91)90366-6.
[21]J. Carlson, V. R. Pandharipande, and R. B. Wiringa, *Variational calculations of resonant states in* ^{4}*He*, Nucl. Phys. A, **424**, pp. 47–59, 1984. DOI: 10.1016/0375-9474(84)90127-1.
[22]B. Borasoy, E. Epelbaum, H. Krebs, D. Lee, and U.-G. Meißner, *Two-particle scattering on the lattice: Phase shifts, spin-orbit coupling, and mixing angles*, Eur. Phys. J. A, **34**, pp. 185–196, 2007. DOI: 10.1140/epja/i2007-10500-9.
[23]B.-N. Lu, T. A. Lähde, D. Lee, and U.-G. Meißner, *Precise determination of lattice phase shifts and mixing angles*, Phys. Lett. B, **760**, pp. 309–313, 2016. DOI: 10.1016/j.physletb.2016.06.081.
[24]M. Pine, D. Lee, and G. Rupak, *Adiabatic projection method for scattering and reactions on the lattice*, Eur. Phys. J. A, **49**, p. 151, 2013. DOI: 10.1140/epja/i2013-13151-3.
[25]S. Elhatisari, D. Lee, U.-G. Meißner, and G. Rupak, *Nucleon-deuteron scattering using the adiabatic projection method*, Eur. Phys. J. A, **52**, no. 6, p. 174, 2016. DOI: 10.1140/epja/i2016-16174-2.
[26]G. Hale, *private communication*, 2008.
[27]S. Quaglioni and P. Navratil, *Ab initio many-body calculations of nucleon-nucleus scattering*, Phys. Rev. C, **79**, p. 044 606, 2009. DOI: 10.1103/PhysRevC.79.044606.
[28]S. Elhatisari, F. Hildenbrand, and U.-G. Meißner, *Ab initio lattice study of neutron–alpha scattering with chiral forces at N3LO*, J. Phys. G, **52**, no. 12, p. 125 102, 2025. DOI: 10.1088/1361-6471/ae2145.
[29]C. Pitrou, A. Coc, J.-P. Uzan, and E. Vangioni, *Resolving conclusions about the early Universe requires accurate nuclear measurements*, Nature Rev. Phys., **3**, no. 4, pp. 231–232, 2021. DOI: 10.1038/s42254-021-00294-6.

[30]H. Meyer, S. Elhatisari, F. Hildenbrand, and U.-G. Meißner, *Elastic deuteron-deuteron scattering within Nuclear Lattice Effective Field Theory*, Jul. 2026. [Online]. Available: https://arxiv.org/abs/2607.00681.
[31]A. N. Tikhonov and V. Y. Arsenin, *Solutions of Ill-Posed Problems*, F. John, Ed. Washington, DC: V. H. Winston & Sons, 1977, p. 258, Distributed by Halsted Press, New York, ISBN: 9780470991244.
[32]W. Meier and W. Glöckle, *Elastic scattering 2 H(d, d) 2 H below 360 keV*, Nucl. Phys. A, **255**, pp. 21–34, 1975. DOI: 10.1016/0375-9474(75)90144-X.
[33]H. M. Hofmann and G. M. Hale, *Microscopic calculation of the He-4 system*, Nucl. Phys. A, **613**, pp. 69–106, 1997. DOI: 10.1016/S0375-9474(96)00418-6.
[34]I. N. Filikhin and S. L. Yakovlev, *Microscopic calculation of low-energy deuteron-deuteron scattering on the basis of the cluster-reduction method*, Phys. Atom. Nucl., **63**, pp. 271–277, 2000. DOI: 10.1134/1.855624.
[35]H. M. Hofmann and G. M. Hale, *He-4 can experiments serve as a database for determining the three-nucleon force?* Phys. Rev. C, **77**, p. 044 002, 2008. DOI: 10.1103/PhysRevC.77.044002.
[36]J. F. Carew, *Deuteron-deuteron elastic and three- and four-body breakup scattering using the Faddeev-Yakubovskii equations*, Phys. Rev. C, **103**, no. 1, p. 014 002, 2021. DOI: 10.1103/PhysRevC.103.014002.
[37]S. A. Afzal, A. A. Z. Ahmad, and S. Ali, *Systematic Survey of the alpha-alpha Interaction*, Rev. Mod. Phys., **41**, pp. 247–273, 1969. DOI: 10.1103/RevModPhys.41.247.
[38]S. Elhatisari, D. Lee, G. Rupak, E. Epelbaum, H. Krebs, T. A. Lähde, T. Luu, and U.-G. Meißner, *Ab initio alpha-alpha scattering*, Nature, **528**, p. 111, 2015. DOI: 10.1038/nature16067.
[39]A. Sarkar, S. Elhatisari, T. A. Lähde, and U.-G. Meißner, *Ab initio α-α scattering with high-fidelity chiral interactions*, Jun. 2026.
[40]S. Elhatisari, F. Hildenbrand, and U.-G. Meißner, *The triton lifetime from nuclear lattice effective field theory*, Phys. Lett. B, **859**, p. 139 086, 2024. DOI: 10.1016/j.physletb.2024.139086.
[41]A. Brinson *et al.*, *Nuclear charge radii of aluminium isotopes at the proton drip line*, May 2026. [Online]. Available: https://arxiv.org/abs/2605.09139.
[42]O. Eizenberg *et al.*, *Nuclear Charge Radius of ^{9}Be from Muonic Atom Spectroscopy Using a Microcalorimeter*, Jul. 2026. [Online]. Available: https://arxiv.org/abs/2607.13690.
[43]Q. Lu, R.-F. Tian, S.-S. Zhang, U.-G. Meißner, and S. Shen, *Deformation effects on reaction observables of beryllium nuclei from ab initio densities*, Aug. 2026. [Online]. Available: https://arxiv.org/abs/2608.18538.
[44]T. Wu, B. Sun, U.-G. Meißner, and S. Shen, *Reaction Cross Sections and α-Cluster Geometry in ^{12}C and Be Isotopes*, Aug. 2026. [Online]. Available: https://arxiv.org/abs/2608.18538.
[45]H. Tong, S. Elhatisari, U.-G. Meißner, and Z. Ren, *Multi-strangeness matter from ab initio calculations*, Sep. 2025. [Online]. Available: https://arxiv.org/abs/2509.26148.